JOURNAL OF CATALYSIS 124, 324–335 (1990)

# Deactivation of Steam-Reforming Model Catalysts by Coke Formation

## I. Kinetics of the Formation of Filamentous Carbon in the Hydrogenolysis of Cyclopentane on $Ni/Al_2O_3$ Catalysts

D. DUPREZ,*,[1] M. C. DEMICHELI,* P. MARECOT,* J. BARBIER,* O. A. FERRETTI,† AND E. N. PONZI†

*Laboratoire de Catalyse en Chimie Organique, UA 350, Université de Poitiers, 40 Avenue du Recteur Pineau, 86022 Poitiers Cédex, France; and †Centro de Investigación y Desarrollo en Procesos Catalíticos, Calle 47 No. 257, La Plata, Argentina

Received July 24, 1989; revised October 19, 1989

Coke formation in the hydrogenolysis of cyclopentane on $Ni/Al_2O_3$ catalysts in the temperature range 300–500°C was studied. A similar change in apparent activation energy for coking obtained with catalysts presenting different surface states coincides with the appearance of filamentous carbon on the catalyst surface. A definite carbon-to-surface nickel ratio seems to be necessary for the nucleation of the filaments. Coked catalysts reveal different activities for hydrogenolysis and hydrogenation reactions depending on the nature of the carbon deposit. The free-metal surface area decreases by two orders of magnitude during coke deposition accompanying cyclopentane hydrogenolysis. Nevertheless, as soon as the filamentous carbon appears on the catalyst, the nickel recovers a significant part of its initial activity, which shows that the accessible fraction of metal increases at the initial stage of the whisker formation. 

## INTRODUCTION

Deactivation of supported metal catalysts by carbon or coke is a serious problem in steam reforming and in other important catalytic processes. The main causes of loss in activity are (i) catalyst sintering, (ii) poisoning by sulfur compounds present in the hydrocarbon feedstock, and (iii) the formation of surface carbonaceous residues. While the effect of sintering and poisoning are relatively well understood, comparatively little is known as yet about the mechanisms by which carbon and/or coke are deposited (*1–3*).

Barbier *et al.* (*4, 5*) have shown that the rate of carbon deposition during cyclopentane reaction on supported platinum catalysts is proportional to the metallic surface area active in the dehydrogenation reaction yielding cyclopentadiene. Hadj-Aissa (*6*) has demonstrated that cyclopentane in an inert atmosphere of nitrogen leads to heavy coke deposits on $Ni/Al_2O_3$ compared with noble metals (Pt, Ir, Rh, Ru, Re) in the temperature range 400–500°C.

The general goal of this work is to study the coke formation, by model molecules, on catalysts with formulations varying from basic $Ni/Al_2O_3$ catalysts to complex multicomponent catalysts for steam reforming. In this paper we investigate how surface properties and metal–support interactions affect the rate and the nature of carbon species deposited from cyclopentane. This molecule was chosen because it can give significant coking rates at relatively low temperatures. Coking experiments were carried out here in a dry atmosphere. The role of water together with the effects of alkali doping will be analyzed in a later paper.

[1]To whom correspondence should be addressed.



0021-9517/90 $3.00

## EXPERIMENTAL

### *Catalyst Preparation*

Catalysts were prepared by an impregnation technique. Eighty grams of Rhône Poulenc SCS-79 δ-alumina was immersed in 200 ml of aqueous solution of $Ni(NO_3)_2 \cdot 6H_2O$. The concentration of the solution was adjusted in order to obtain either 2 or 10 wt% of nickel in the catalyst oxides.

Water was evaporated under reduced pressure (13 kPa) and the precursor was dried in air at 110°C for 16 h and subsequently heated at 1°C $min^{-1}$ in an air flow to 400°C: this operational sequence defines the "standard" pretreatment. The total amount of the 10% Ni catalyst was divided into two parts, one of them being calcined in static air at 700°C for 18 h in order to induce $Ni-Al_2O_3$ interactions. These catalysts are referred to as Ni*X*AC*Y*, where *X* is the nickel content and *Y* the calcination temperature (omitted for catalysts under standard pretreatment). Values of BET surface area for each catalyst are listed in Table 1.

### *Activation and Coking Reaction*

Reduction of the catalyst and the subsequent coking reaction were performed *in situ* in a conventional flow reactor consisting of a Pyrex–glass tube (16 mm i.d.) in which a sintered glass disk was welded to support the catalyst. The temperature was measured by a chromel–alumel thermocouple placed in the center of the catalyst bed. The catalyst was first heated at 1°C $min^{-1}$ under flowing hydrogen (26 ml g $Ni^{-1}$ $s^{-1}$) to 500°C and allowed to remain at that temperature for 10 h. Afterward, the catalyst was cooled to the reaction temperature and hydrogen was replaced by the coking mixture consisting of cyclopentane diluted with hydrogen or nitrogen. Experiments were carried out in the temperature range 300–500°C with molar flow rates of 0.0247 mol $h^{-1}$ for cyclopentane, 0–0.494 mol $h^{-1}$ for hydrogen, and 0–0.0576 mol $h^{-1}$ for nitrogen and with a catalyst weight of 0.05–0.3 g. Gases were purified by passing through conventional deoxo-zeolite traps. Cyclopentane of analytical grade containing less than 1% of 2,2-dimethylbutane as main impurity was utilized. Gaseous reaction products were analyzed by FID gas chromatography on a 25-m capillary column of $Al_2O_3$ (0.32 mm i.d., film thickness 3 μm) at 100°C with hydrogen as carrier gas at a flow rate of 15 ml $min^{-1}$.

For the transformation of cyclopentane with hydrogen, two main reactions are postulated to occur, namely, the hydrogenolysis reaction (essentially to methane)

$$\text{cyclo-}C_5H_{10} + 5H_2 \rightarrow 5CH_4; \quad \Delta H_{700\,K} = -346 \text{ kJ mol}^{-1} \quad (1)$$

and the coking reaction

$$\text{cyclo-}C_5H_{10} \rightarrow 5CH_x + 10(1 - x/2)H_2; \quad \Delta H_{700\,K} = +192 \text{ kJ mol}^{-1} \quad (\text{for } x = 0) \quad (2)$$

### *Metal Surface and Metal Reduction Measurements*

Metal surface and metal reduction parameters were determined using a pulse chromatographic system described elsewhere (*7*). The catalyst was first reduced under the above-described conditions and then purged in flowing argon for 3 h at 500°C. Chemisorption of hydrogen was undertaken at room temperature (pulses of 0.245 ml every minute) to determine the irreversible hydrogen uptake. After temperature-programmed desorption at 4°C $min^{-1}$ in flowing argon up to 500°C, the oxygen uptake (pulses of 0.245 ml every minute) was measured at that temperature. The amount of chemisorbed hydrogen was referred to the metal loading in the quantity $H_c/Ni_T$ (atoms of H chemisorbed/total nickel atoms). The degree of

TABLE 1

BET Surface Area ($S_t$) of the Catalysts

| Catalyst | Ni (wt%) | $S_t$ ($m^2$ $g^{-1}$) |
|---|---|---|
| Ni2AC | 2.3 | 82 |
| Ni10AC | 8.81 | 75 |
| Ni10AC700 | 10.41 | 49 |

nickel reduction, $\%R_c$, was evaluated from the oxygen uptake capacity $O_c$ determined at 500°C. Assuming that $O/Ni_R = 1.1$ ($Ni_R$ indicates reduced nickel), we obtain $\%R_c = 90.9\ O_C/Ni_T$ (*7*). Dispersity, $\%D_C$, is estimated from $\%D_C = 222\ H_c/O_C$, which is in good agreement with values resulting from magnetic measurements (*7*). Finally, the particle size was calculated from $d_C = 978/\%D_C$, based on an equidistribution of the low index faces {111}, {110}, and {100} at the surface of the metallic particles.

*Scanning Electron Microscopy (SEM)*

Samples consisting of a few particles of coked catalysts were fixed into a silver glue spread on sample holders. A gold layer, 15–20 nm thick, was introduced by sputtering pure gold at 13 Pa. These specimens were studied in a JEOL 35 CF electron microscope.

*Temperature-Programmed Oxidation*

Samples of fresh coked catalyst were oxidized under a flow of 2% oxygen in helium at 7°C $min^{-1}$ in a pulse-chromatographic system using a Porapak-Q column. The quantity of carbon deposited was deduced from the amount of $CO_2$ produced during the temperature-programmed combustion (*5*). Under our experimental conditions no production of CO was detected.

## RESULTS

*Activation and Surface Properties*

Table 2 shows that dispersity and metal surface area, $S_m$, are strongly reduced with increasing temperature; this is due to a partial formation of bulk aluminates by interaction between nickel and aluminium oxide, as confirmed by X-ray diffractometry. These aluminates of spinel structure are hardly reduced in hydrogen at temperatures lower than 800°C (*8*), which induces a significant decrease of the oxygen uptake at 500°C. Average particle sizes deduced from chemisorption data, $d_C$, are compared to those estimated using Scherrer's equation for X-ray line broadening (hexagonal NiO (012) reflexion) $d_X$, in the last two columns of Table 2. The difference between $d_C$ and $d_x$ found for Ni10AC700 is attainable since its Ni particles probably become polycrystalline after calcination at 700°C. Similar effects have been reported in the literature for steam reforming (*1*).

*Temperature Dependence of the Coke Deposition*

In Fig. 1 the amount of coke deposited during the first hour of reaction is plotted versus $1/T(K)$ for Ni2AC at $H_2/CPA = 0$ (CPA is cyclopentane), for Ni10AC at $H_2/CPA = 1.75$, and for Ni10AC700 at different $H_2/CPA$ ratios. As soon as the temperature or carbon content goes further than the point marked B, there is, in all cases, an abrupt change in the apparent activation energy for coke deposition (global carbon contents are proportional to average rates of coke deposition between 0 and 1 h). For Ni10AC700 the B-point shifts to higher temperatures when the $H_2/CPA$ ratio is increased, even though the carbon content at $T_B$ remains approximately the same. Comparatively,

TABLE 2

Metal Surface Parameters in the Reduced Catalysts at 500°C

| Catalyst | Nickel loading ($\mu$mol $g^{-1}$) | $H_C/Ni_T$ | $\%R_C$ | $\%D_C$ | $S_m$ ($m^2\ g^{-1}$) | $d_C$ (nm) | $d_X$ (nm) |
|---|---|---|---|---|---|---|---|
| Ni2AC | 392 | 0.135 | 79 | 34 | 5.4 | 2.9 | — |
| Ni10AC | 1501 | 0.085 | 95 | 18 | 11 | 5.4 | 6.0 |
| Ni10AC700 | 1773 | 0.010 | 37 | 5.4 | 3.9 | 18.1 | 7.4 |

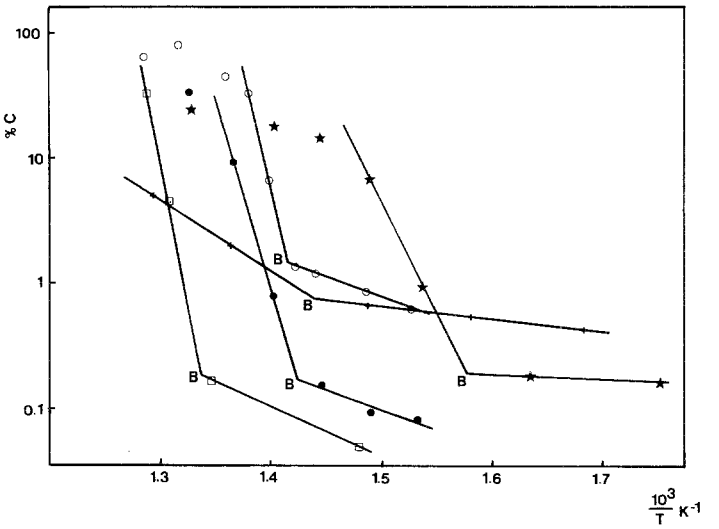


FIG. 1. Temperature dependence of coke deposition on: Ni2AC: (+) $P_{CPA}$ = 30 kPa, $P_{N_2}$ = 70 kPa, $H_2$/CPA = 0; Ni10AC: (○) $P_{CPA}$ = 36 kPa, $P_{H_2}$ = 64 kPa, $H_2$/CPA = 1.75; Ni10AC700: (★) $P_{CPA}$ = 30 kPa, $P_{N_2}$ = 70 kPa, $H_2$/CPA = 0; (●) $P_{CPA}$ = 36 kPa, $P_{H_2}$ = 64 kPa, $H_2$/CPA = 1.75; (□) $P_{CPA}$ = 5 kPa, $P_{H_2}$ = 95 kPa, $H_2$/CPA = 20.

Ni2AC and Ni10AC allow more coke to be formed before the rupture occurs. Below the B-point all apparent activation energies range from 20 to 80 kJ $mol^{-1}$. The breaking at B-point in the Arrhenius plot of Fig. 1 was shown to correspond with the appearance of filamentous carbon on the catalysts. This is clear from SEM micrographs obtained with catalyst samples coked below and above the B-point, as seen in Fig. 2 for Ni10AC. This was also observed with Ni10AC700. However, filaments could not be detected on coked samples of Ni2AC, even at 500°C.

*Reactivity of Coke Deposits*

Freshly coked samples of the different catalysts were characterized by temperature-programmed oxidation performed up to 900°C to burn completely the coke formed.

A series of TPO curves for reaction of the coke deposited with oxygen, as a function of coking temperature, are presented in Figs. 3 to 5. Three aspects appear to be common to all catalysts:

(1) when coking is carried out under conditions falling below the B-point (see Fig. 1), a reactive species (I) is formed with a peak temperature, $T_{pI}$ = 350 ± 20°C. This species would correspond to carbon and/or coke deposited on the nickel surface.

(2) When the experiments are performed far above the B-point, a highly nonreactive form (III) is observed at temperatures, $T_{pIII}$ = 650 ± 50°C. Such a form is associated with a graphitic carbon like that which forms the outer shell of carbon filaments.

(3) Finally, under coking conditions falling just over the B-point a third species (II) is determined with a peak temperature, $T_{pII}$ = 450 ± 20°C. This intermediate form is believed to be formed by migration of carbon atoms from the metal to the support.

The II-type carbon is detected particularly well for Ni2AC and Ni10AC700, both catalysts having an important nickel–support interaction: This happened with Ni2AC (in spite of its high dispersion) and with Ni10AC700 as the consequence of the formation of bulk aluminates, as was confirmed

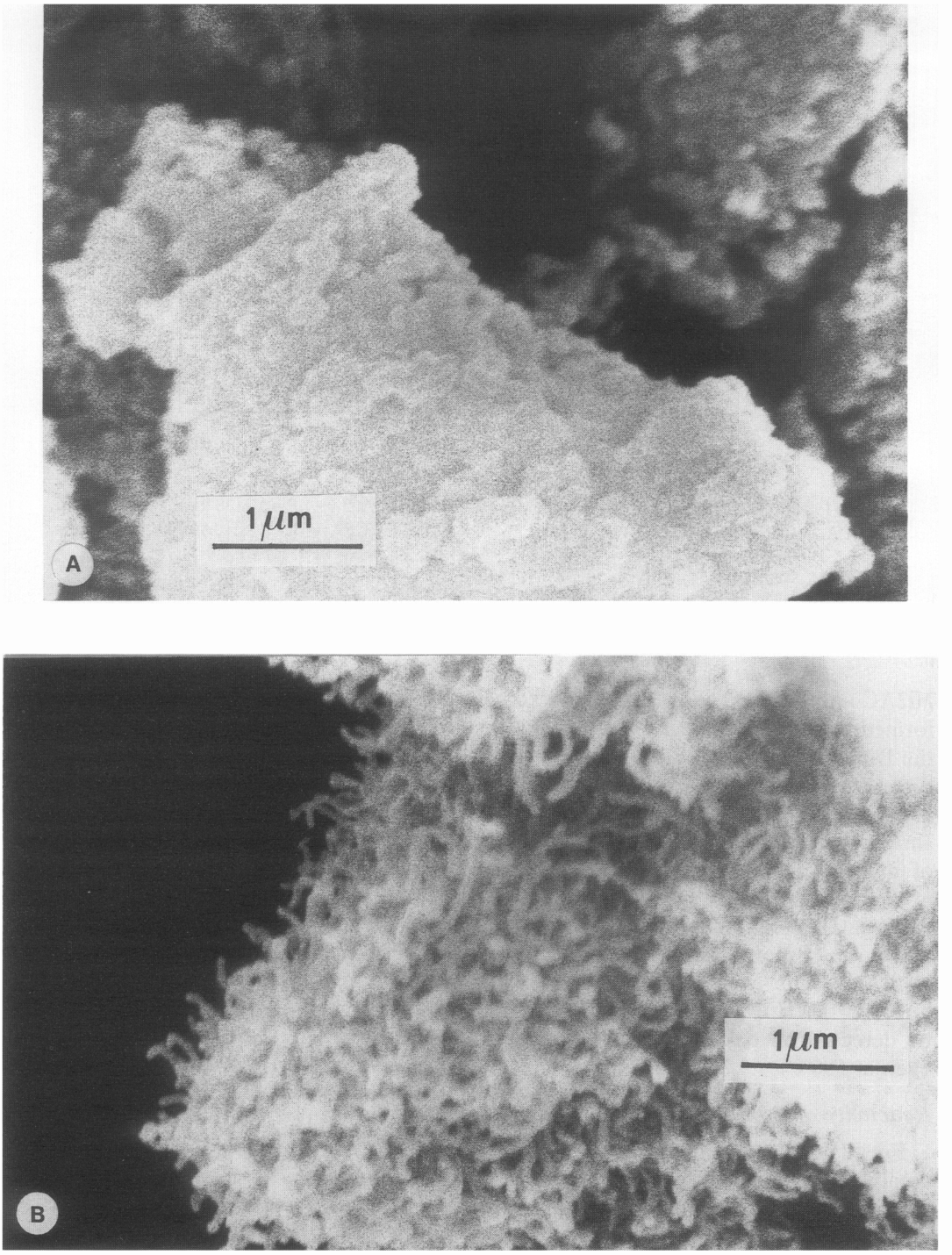


FIG. 2. Electron micrographs of coked Ni10AC. (A) 1 h coking at 430°C, $H_2$/CPA = 1.75. (B) 1 h coking at 450°C, $H_2$/CPA = 1.75.

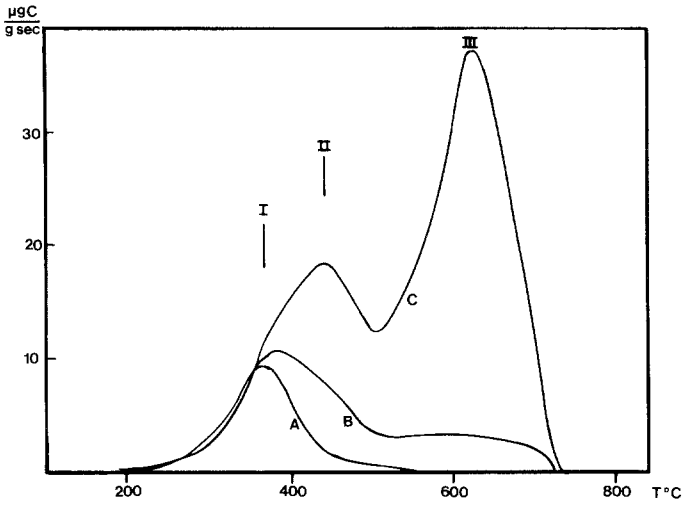


FIG. 3. TPO profiles of coke deposited on Ni10AC at (A) 430°C, (B) 450°C, and (C) 460°C; $H_2$/CPA = 1.75; reaction time = 1 h.

by X-ray analysis. However, for Ni10AC, a partial superposition between types I and II is observed.

*Catalytic Activity in Hydrogenolysis*

Even when temperature and $H_2$/CPA ratio were varied, the main product was, most often, methane, demonstrating that cyclopentane is irreversibly adsorbed and decomposed on nickel with a complete breakage of carbon–carbon bonds (*9*). Table 3 shows a typical chromatographic analysis of the products. In comparison with platinum, the yield in gaseous products of dehydrogenation, i.e., cyclopentane, cyclopentadiene, etc., is negligible. Figure 6 shows the total

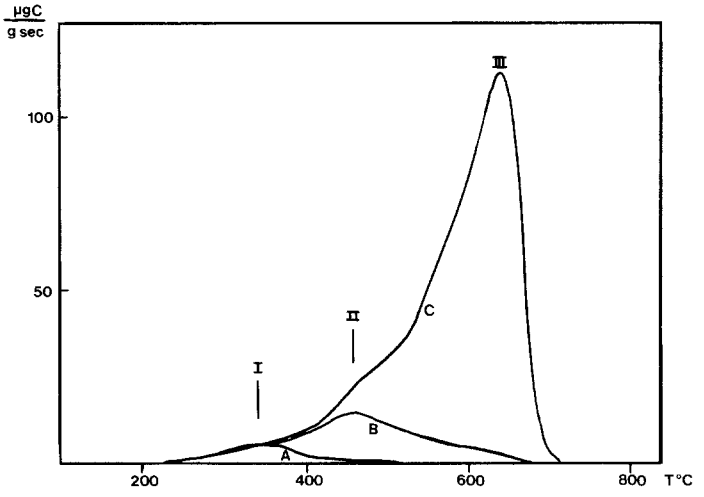


FIG. 4. TPO profiles of coke deposited on Ni10AC700 at (A) 340°C, (B) 380°C, and (C) 420°C; $H_2$/CPA = 0; reaction time = 1 h.

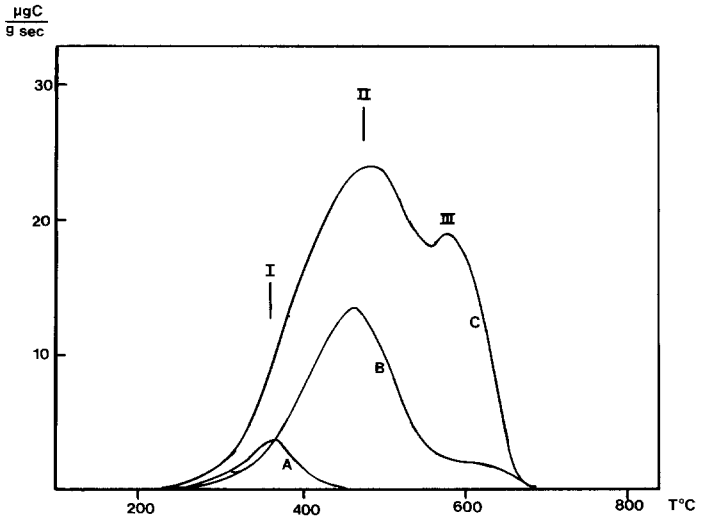


FIG. 5. TPO profiles of coke deposited on Ni2AC at (A) 340°C, (B) 460°C, and (C) 500°C; $H_2$/CPA = 0; reaction time = 1 h.

conversion of cyclopentane at selected temperatures above and below the breakpoint. At temperatures lower than $T_B$ the consumption of cyclopentane declines more or less rapidly, depending on the hydrogen pressure. On the contrary, at temperatures above $T_B$, the initial diminution is followed by a growth of conversion, all the experiments producing a maximum at a given time. This increment in conversion is ascribed to the formation of whisker carbon. It is well-documented that this type of carbon does not deactivate the catalyst (*10*). Moreover, we will see further that above the B-point, the catalyst recovers a large part of its accessible metal area. This effect is not observed at the lower temperatures (below the B-point) where filament formation would not take place and a "coke" of a different nature deactivates the catalyst.

TABLE 3

Typical Composition of Gaseous Products in Coking Experiments (Ni10AC, 440°C, $H_2$/CPA = 1.75)

| Time on stream (h) | $C_1$ | $C_2$ | $C_3$–$C_5$ | CPA | CPE[a] | CPD[a] |
|---|---|---|---|---|---|---|
| 0.07 | 21.3 | 0.09 | 0.03 | 78.4 | 0.21 | 0.02 |
| 0.92 | 6.9 | 0.06 | 0.03 | 92.8 | 0.20 | 0.03 |

[a]CPE indicates cyclopentene, CPD indicates cyclopentadiene.

### *Change in the C/$Ni_s$ Ratio during Hydrogenolysis and Coking*

In the previous analysis (Fig. 1) we found that, for Ni10AC700, the locus of the B-point was influenced by the $H_2$/CPA ratio. Evidently the critical carbon content necessary for the nucleation of carbon filaments depends not only on catalytic activity but also on the intrinsic rates of reactions (1) and (2), as they present orders in hydrocarbon and/or hydrogen different from zero (*11*, *12*). Indeed, selectivities of both reactions are clearly modified when $T_B$ is exceeded, as seen from values given in Table 4 for Ni10AC700 at different $H_2$/CPA ratios.

Accounting for the different values of carbon content found at $T_B$, in Fig. 7, the number of carbon atoms deposited by each surface nickel atom, C/$Ni_s$, is plotted against the temperature. It is observed that except

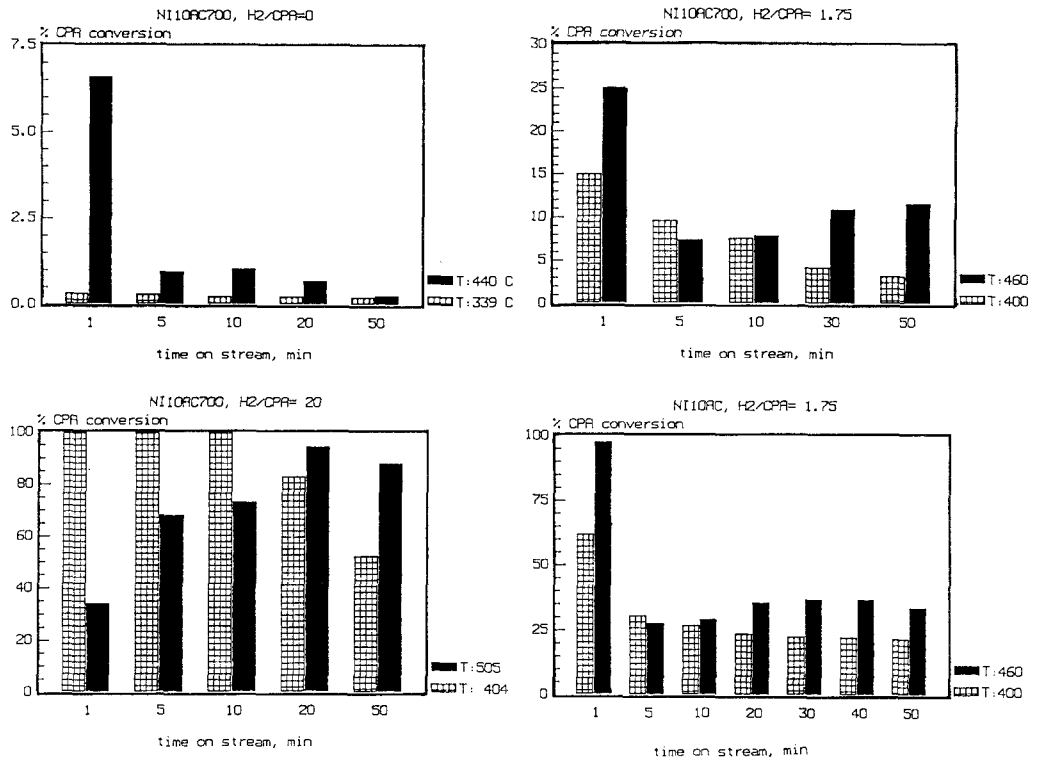


FIG. 6. Conversion of cyclopentane during coking experiments on Ni10AC700 (different $H_2$/CPA ratios) and Ni10AC (see Fig. 1).

TABLE 4

Selectivity for Hydrogenolysis of Cyclopentane (CPA) and Coking for Ni10AC700 at Different $H_2$/CPA Ratios

| $H_2$/CPA | Temperature (°C) | TTG[a] (%) | $S_C$[b] (%) | $S_H$[b] (%) |
|---|---|---|---|---|
| 0 | 248 | 0.29 | 7.4 | 92.6 |
| ($T_B$ = 375°C) | 339 | 0.27 | 9.0 | 91.0 |
| | 378 | 0.47 | 25 | 75 |
| 1.75 | 398 | 7.1 | 0.2 | 99.8 |
| ($T_B$ = 437°C) | 419 | 4.8 | 0.6 | 99.4 |
| | 440 | 3.1 | 5.1 | 94.9 |
| 20 | 404 | 74 | — | 100 |
| ($T_B$ = 482°C) | 470 | 88 | — | 100 |
| | 495 | 94 | 1 | 99 |

[a]TTG, total conversion of CPA.

[b]$S_H$, $S_C$, selectivities for the hydrogenolysis and the coking reactions.

for Ni2AC, a value between 8 and 9 is always obtained before the break-point is detected.

### *Change in the Free-Metallic Surface Area during Hydrogenolysis and Coking*

We have shown that, with increasing temperatures, the $C/Ni_s$ ratio grew to a value of 8–9 and, after that, carbon filaments appeared on the catalysts. It was interesting to evaluate the free-metal surface area for catalyst samples, with or without filaments.

Accordingly, catalytic activities for hydrogenolysis of cyclopentane and hydrogenation of benzene, which are typical examples of structure-sensitive and nonstructure-sensitive reactions, respectively, were measured on Ni10AC700 coked below and above the B-point. Figure 8 shows the program followed. After normal reduction, a primary hydrogenolysis of cyclopentane, during which coke is deposited, is carried

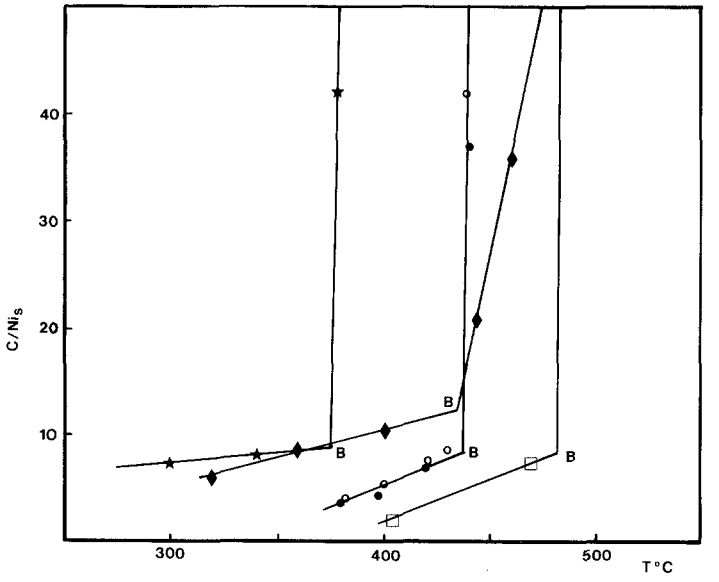


FIG. 7. Evolution of the C/Ni$_s$ ratio during hydrogenolysis and coking on: Ni2AC: (◆) $H_2$/CPA = 0; Ni10AC: (○) $H_2$/CPA = 1.75; Ni10AC700: (★) $H_2$/CPA = 0, (●) $H_2$/CPA = 1.75, (□) $H_2$/CPA = 20 (slopes above the B-point are based on data out of the limits of the diagram).

out at temperatures below and above the B-point; then the catalyst is quenched, either to 250°C to perform a secondary hydrogenolysis or to 180°C to carry out the hydrogenation of benzene. Both reactions were checked; neither produced coke on a fresh catalyst at these temperatures.

Calculated values of reaction rate and activity for these reactions on fresh and coked catalyst samples are compared in Table 5. It is seen that while the reaction rate is drastically reduced by the coke formed at 420°C (below the B-point), nickel having formed filamentous carbon still conserves a nonnegligible level of activity. Indeed, the hydrogenolysis of cyclopentane seems to be more

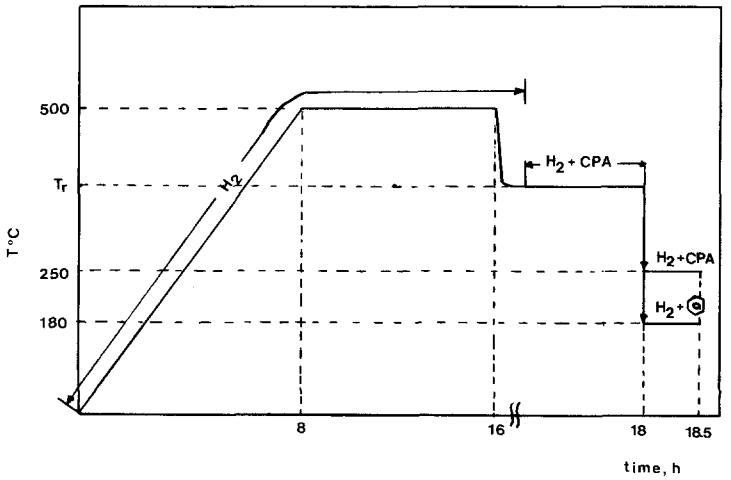


FIG. 8. Experimental sequence.

TABLE 5

Activity of Coked Ni10AC700 in Structure-Sensitive and Nonstructure-Sensitive Reactions[a]

| Catalyst | Hydrogenolysis of CPA 250°C | | Hydrogenation of benzene at 180°C | |
|---|---|---|---|---|
| | Reaction rate $10^3$ mol $h^{-1}$ $g^{-1}$ | Normalized activity (coked/fresh) | Reaction rate $10^3$ mol $h^{-1}$ $g^{-1}$ | Normalized activity (coked/fresh) |
| Fresh | 15 | 1 | 41 | 1 |
| Coked 1 h, 420°C | 0.25 | 0.016 | 2.6 | 0.05 |
| Coked 1 h, 480°C | 2.5 | 0.16 | 13 | 0.32 |

[a]Activity values are calculated from CPA conversion, stabilized after 30 min on-stream.

affected, presumably owing to the disappearance of specific active centers caused by filament growth.

These results seem to show that the accessible fraction of the nickel surface area first decreases along with coke deposition and then increases as soon as the filaments of carbon begin to appear.

## DISCUSSION

The present study shows that cyclopentane reacts on $Ni/Al_2O_3$ yielding carbon and methane, the latter being the main product of hydrogenolysis. An abrupt change in the apparent activation energy for coking (B-point in Fig. 1) is proved to correspond to a change in the morphology of the deposits from surface or subsurface carbon to filamentous carbon, as was observed by electron microscopy. The break-point appeared to be affected by kinetic and other aspects, i.e., temperature and partial pressures and thermodynamic requirements; in other words a definite concentration of carbon on nickel (eight to nine carbon atoms per surface nickel atom) is necessary for the filaments of carbon to appear. Neither the particle size nor metal–support interactions seem to affect the $C/Ni_s$ ratio at break-point B. It has also been shown that filamentous carbon leads to a higher residual activity in hydrogenolysis compared to the more toxic carbon deposited at temperatures lower than $T_B$. This higher activity is also evident in structure-insensitive reactions like hydrogenation of benzene. These results show that the free-metal surface area of nickel is higher in the domain of filamentous carbon than in the domain of low-temperature carbon formation. This increase in the free-metal surface area may be the consequence of a change in the rate-determining step (rds) of the hydrogenolysis reaction, i.e., the rate of the gasification of adsorbed hydrocarbon fragments with hydrogen becomes higher than the rate of hydrocarbon adsorption as the temperature is raised (*10*). Nevertheless, this observation is concomitant with the appearance of whisker carbon, inducing us to think that the increase in the metal accessibility is also due to a redistribution of the carbon on the particle.

It has been reported earlier that metastable nickel carbides are involved in the decomposition of hydrocarbons on nickel surfaces. Renshaw *et al.* (*13*) observed the formation of an intermediate carbide phase prior to carbon formation at temperatures as high as 550°C. Manning *et al.* (*14*) reported that the actual equilibrium of carbon formation on nickel requires higher concentrations of $CO_2$, $H_2$, and $CH_4$ than if one assumed $\beta$-graphite were formed. They proposed that carbon formation occurs via an intermediate carbide which continuously decomposes into graphite and nickel. Recently, De Bokx *et al.* (*15*) have also observed deviation from graphite equilibria in

the carburization of silica-supported nickel and iron catalysts by methane and carbon monoxide. By thermomagnetic analysis, these authors (*16*) studied both transient and steady-state behavior in the carburization of a nickel catalyst by methane under conditions at which carbon filaments were formed. Accounting for the initial decrease in magnetization observed (75% of the initial value) they assumed that high carbide contents precede the nucleation of carbon. They proposed that a bulk carbide is formed at this stage. As the magnetization is partially recovered after 18 h on stream they designed experiments tending to examine the steady-state carburization. By measuring the reversible loss of magnetization produced during carburization–hydrogenation cycles they concluded that a substoichiometric bulk carbide is present under conditions of filament growth. In a recent paper, Alstrup (*17*) criticized the interpretation of magnetic measurements carried out by De Bokx and co-workers (*15*) in stating that the loss of about 75% of the magnetic moment in the nickel particles in the beginning of their carburization experiments corresponds not to the formation of bulk nickel carbides, but to the passivation of the moments of the outer shells in the "induction period" before the nucleation of the filament. Based on studies of interaction of methane with single nickel surfaces, he hypothesized the formation of a surface carbide which would form the source for carbon diffusion into the particle.

In the present study, if the formation of a bulk nickel carbide was, similarly, a required condition to start the growth of carbon filaments, we should expect to obtain the break-point at the same value of $C/Ni_r$ (that is, reduced nickel) rather than $C/Ni_s$. Assuming that the amount of reduced nickel is not increased during the reaction, the results presented in Table 6 indicate that this is not the case. On the contrary, this shows that a definite state of the catalyst surface, involving most probably a surface carbide as well as multilayers of free carbon, is present during the induction period preceding the nucleation of filaments. The migration of part of that carbon to the nearest support should not be disregarded.

TABLE 6

$C/Ni_r$ versus $C/Ni_s$ at the Break-Point (B-Point)

| Catalyst | *D%* | $C/Ni_r$ | $C/Ni_s$ |
|---|---|---|---|
| Ni10AC | 17.9 | 1.57 | 8.75 |
| Ni10AC700 | 5.4 | 0.46 | 8.5 |
| Ni2AC | 34.0 | 3.74 | 11 |

It seems important, at this point, to emphasize the crystallographic specificity for chemisorption and carbon formation, which proceed preferentially on (100) and (110) nickel faces (*18, 19*) and for graphite segregation, permitted on (111) and (311) faces (*20*). All these processes, being sustained by a resultant driving force (concentration and/or temperature gradient) (*19*), provoke the reconstruction of the particle, with some action on its catalytic properties as seen for hydrogenolysis and hydrogenation reactions.

*Well-Dispersed Ni2AC Catalyst*

The higher value of $C/Ni_s$ before the break-point, together with the lower apparent activation energy above that point observed for this catalyst, can be explained by the smaller size of its particles (average particle diameter, $d = 3$ nm) and this is in agreement with the less abundant III species observed for Ni2AC in Fig. 5. In fact it was reported (*16*) that a minimum diameter of about 10 nm together with a high carbide content is necessary for nucleation of carbon. Only then will a reduced fraction of particles of the Ni2AC catalyst produce carbon filaments.

The intermediate carbon form II, with a peak temperature of 450°C, is associated with nickel–alumina interactions like formation of nonstoichiometric aluminates which could lodge and stabilize carbon.

Since the small particles are not able to produce a filament, they remain attached to the support and become easily encapsulated by the growing carbon.

## CONCLUSIONS

The studies show that two different domains are found in the transformation of cyclopentane on $Ni/Al_2O_3$: at low temperature a slow evolution of the coking rate with simultaneous deactivation of the hydrogenolysis reaction is followed by a significant acceleration of the coke deposition, characterized by the appearance of carbon filaments as soon as a certain temperature is surpassed (B-point). The temperature of this break-point essentially depends on hydrogen concentration which tends to retard the appearance of the filaments. Nevertheless, whiskers are developed only after a definite carbon-to-surface nickel ratio (equal to 8–9) is attained and for catalysts with an average particle diameter of at least 6 nm.

In the low-temperature zone (below the B-point) the accessible nickel area decreases by about two orders of magnitude. When the temperature just exceeds $T_B$, the accessible nickel area grows, achieving roughly 30% of its initial value. This increase in the accessible nickel area appears to be linked to two different causes, namely, a change in the rds of the hydrogenolysis reaction and a redistribution of the surface carbon required for nucleation of filamentous carbon.

The formation of a surface carbide seems to be involved during the induction period after the nucleation of filaments. The relative excess of carbon determined at the B-point is attributed to the formation of carbon multilayers and migration of this carbon to the adjacent support.

## ACKNOWLEDGMENTS

This study was performed in the framework of an International Programme of Scientific Cooperation (PICS) sponsored by the CNRS and the CONICET, and both are gratefully acknowledged.

## REFERENCES

1. Rostrup-Nielsen, J. R., *in* "Catalysis, Science and Technology" (J. R. Anderson and M. Boudart, Eds.), Vol. 5, p. 77. Springer, Berlin 1984.
2. Bartholomew, C. H., *Catal. Rev.-Sci. Eng.* **24,** 67 (1982).
3. Jackson, S. D., Thomson, S. J., and Webb, G., *J. Catal.* **70,** 249 (1981).
4. Barbier, J., Churin, E., Parera, J. M., and Rivière, J., *React. Kinet. Catal. Lett.* **28,** 245 (1985).
5. Barbier, J., *Appl. Catal.* **23,** 225 (1986).
6. Hadj-Aissa, M., Thesis, Poitiers 1987.
7. Duprez, D., Mendez, M., and Dalmon, J. A., *Appl. Catal.* **21,** 1 (1986).
8. Zielińsky, J., *J. Catal.* **76,** 157 (1982).
9. Schouten, F. C., Gijzeman, O. L. J., and Bootsma, G. A., *Surf. Sci.* **87,** 1 (1979).
10. Rostrup-Nielsen, J. R., "Steam Reforming Catalysts." Danish Technical Press, Copenhagen, 1975.
11. Trimm, D. L., *Catal. Rev.-Sci. Eng.* **16,** 155 (1977).
12. Dalmon, J. A., and Martin, G. A., *J. Catal.* **66,** 214 (1980).
13. Renshaw, G. D., Roscoe, C., and Walker, P. L., *J. Catal.* **18,** 164 (1970).
14. Manning, M. P., Garmirian, J. E., and Reid, R. C., *Ind. Eng. Chem. Process Des. Dev.* **21,** 404 (1982).
15. De Bokx, P. K., Kock, A. J. H. M., Boellaard, E., Klop, W., and Geus, J. W., *J. Catal.* **96,** 454 (1985).
16. Kock, A. J. H. M., De Boks, P. K., Boellaard, E., Klop, W., and Geus, J. W., *J. Catal.* **96,** 468 (1985).
17. Alstrup, I., *J. Catal.* **109,** 241 (1988).
18. Audier, M., Oberlin, A., and Coulon, M., *J. Cryst. Growth* **55,** 549 (1981).
19. Audier, M., Coulon, M., and Oberlin, A., *Carbon* **19,** 217 (1981).
20. Yang, R. T., and Chen, J. P., *J. Catal.* **115,** 52 (1989).